On the Design of Recuperator for Transcritical Cycle Adopting CO₂-Based Mixture as Working Fluid: A Focus on Transport Properties Prediction

Michele Doninelli* and Gioele Di Marcoberardino

Transcritical cycles working with CO₂-based mixtures gain considerable attention due to thermodynamic efficiency gain compared to pure sCO₂ in hot environments. Previous literature works prove that the adoption of CO₂ mixtures provides a reduction of the levelized cost of electricity in concentrated solar power applications and medium–high temperature heat recovery. However, for techno-economic analysis and heat exchanger design, proper evaluation of transport properties of the CO₂-based mixtures in power cycle conditions is necessary. Herein, it deals with the analysis of the proper transport properties models for CO₂ mixtures to assess their actual thermal behavior. A literature review on transport properties models, and their validation with available experimental data, proves that the friction theory is suitable for CO₂ blended with dopants having high molecular complexity. The impact of the different model selection on the recuperator sizing, considering optimized power cycle conditions, is assessed on the CO₂ mixtures with hexafluorobenzene and decane: The TRAPP and Chung–Lee–Starling models are imported from Aspen Plus, while the friction theory model is implemented and calibrated in an in-house MATLAB code. The optimal design of the recuperator for the $CO_2 + C_6F_6$ mixture in a 100 MW$_{el}$ power block coupled with a solar power plant located in Sevilla is carried out.

1. Introduction

The EU aims to be climate neutral within 2050 with a long-term strategy, and there is need for high-efficient technologies to meet such ambitious goal. In this context, concentrating solar power (CSP) is one of the most attractive technologies since it can provide dispatchable electricity to the grid when coupled with thermal energy storage (TES) system, although a large-scale development is limited by significant capital costs, which negatively affect the levelized cost of electricity (LCOE).

CSP is expected to deliver up to 12% of the global electricity by year 2050.[1] To achieve this ambitious goal, many programs have been launched from Europe (H2020) and the United States (SunShot) aiming at achieving higher power block thermal efficiencies and lowering capital costs. Particular attention is given to alternative working fluids in order to reduce the system complexity and size. Supercritical CO₂ power cycles are expected to be the primary choice for next-generation power plants, but they are penalized by dry cooling in high-temperature environments, typical of CSP locations. In fact, at high values of minimum cycle temperature, the benefit related to the exploitation of real gas effect is mitigated. The H2020 SCARABEUS project[2] introduced the adoption of innovative CO₂ mixtures, using dopants with higher critical temperature than CO₂, allowing transcritical Rankine cycles even in hot and arid regions, then exploiting the benefit of liquid-phase compression. As additional benefit, CO₂ mixtures typically possess good thermodynamic efficiency even in a simple-recuperated layout, thus requiring less components and minor management complexity in comparison with a recompressed sCO₂ cycle. The adoption of CO₂ mixtures could be advantageous also in the medium–high temperature heat recovery applications.[3] The temperature glide occurring during mixture's condensation could be exploited for cogeneration scopes, such as the CO₂ mixture with hexafluorobenzene (C_6F_6), has been extensively studied both theoretically[4,5] and experimentally[6] as innovative working fluid in CSP tower plant with 550 °C turbine inlet temperature, with solar salts as heat transfer fluid. Many other dopants have been considered in the high-temperature CSP context, such as SO₂,[7] TiCl₄, and N₂O₄,[8] and even if CO₂ mixtures have been investigated from the thermodynamic point of view, no studies have been carried out in the nonequilibrium field. On the contrary, the relevance of transport properties in heat exchangers design and rating, as well as in the transient behavior of the mixture, is well recognized, and this work is intended to provide insight into the appropriate modeling of viscosity and thermal conductivity of CO₂ mixtures in power cycle conditions.

M. Doninelli, G. Di Marcoberardino
Dipartimento di Ingegneria Meccanica ed Industriale
Università degli Studi di Brescia
via Branze, 38, 25123 Brescia, Italy
E-mail: m.doninelli002@unibs.it

The ORCID identification number(s) for the author(s) of this article can be found under https://doi.org/10.1002/ente.202300677.

Many experimental dynamic viscosity data are available for mixtures of carbon dioxide with impurities involved in the carbon capture and storage (CCS) processes, as well as with methane due to industrial interest in natural gas. Li et al.[9] collected experimental data of CO_2-rich mixtures with impurities relevant for CCS and validated the most adequate models for that purpose. Nazeri and Chapoy[10] tested the viscosity of several CO_2-rich mixtures and recommended the most appropriate models to be adopted, but the study regarded only CO_2 mixtures with lightweight and simple components involved in CCS processes. In contrast, in the application of interest here, the dopant to be mixed with CO_2 is typically a compound characterized by high molecular complexity, which helps to balance the heat capacities within the recuperator. Due to this literature gap, this work is aimed to assess the appropriate transport properties models for CO_2 mixtures with complex compounds. Few experimental viscosities and thermal conductivities of CO_2 mixtures with heavy and complex hydrocarbons, from enhanced oil recovery sector, proved fundamental to validate the reliability of the investigated models in the next sections. The scarcity of experimental thermal conductivity data highlights the need to perform more experimental activity in this field.

It is worth to mention that the adoption of transcritical CO_2-based cycles was proven to be an interesting solution not only for power generation purposes but also for energy storage systems. In fact, Liu et al.[11] proposed a two-stage transcritical compressed CO_2 energy storage system that outperforms conventional compressed air energy storage in terms of overall efficiency. The adoption of transcritical CO_2-based mixtures instead of pure CO_2 could provide further advantages, and the present paper provides useful guidelines to model transport properties for components design and rating.

In the first section, several transport properties models available from the literature that are capable of describing both dense liquid and vapor phases are briefly presented. Afterward, the comparison with few experimental data in high-density conditions indicates that the recent friction theory model has improved ability to reproduce transport properties of dense CO_2 complex mixtures compared to conventional one-fluid theories. Then, the friction theory models for viscosity and thermal conductivity have been optimized for two mixtures of interest of this work. Specifically, the dopants considered here are hexafluorobenzene (C_6F_6) that has been extensively investigated as promising dopant in previous works and n-decane ($C_{10}H_{22}$) because it is a heavy and complex compound (as C_6F_6) with CO_2 mixture transport property data available in literature in a wide range of pressures and temperatures. Thus, the primary interest of this work is the transport property characterization of the CO_2/C_6F_6 mixture, then the $CO_2/C_{10}H_{22}$ is primarily investigated to assess the influence of the model selection on a mixture whose transport properties are well known. Once assessed that the friction theory models for viscosity and thermal conductivity have superior predictivity in complex mixtures compared to other literature models available in commercial software, the coefficients required by the friction theory models are regressed for the mixtures investigated, and the influence of the transport model used is studied in real case studies. The CO_2/C_6F_6 mixture is applied as working fluid in a concentrated power plant with solar salt as heat transfer fluid (HTF), then 550 °C as maximum cycle temperature, a

thermal level compatible with the thermal stability of the fluid.[6] The $CO_2/C_{10}H_{22}$ mixture is simulated in a concentrated solar plant with parabolic through, with maximum cycle temperature equal to 350 °C, compatible with the state-of-the-art thermal oil level (around 390 °C). The composition and the operating conditions are optimized for the considered case studies. Then, the printed circuit heat exchanger (PCHE) recuperator has been designed with different transport property methods to highlight their influence on the size prediction and to assess whether a method easily available from commercial software could be suitable for this scope and then for a realistic cost assessment and sizing. The PCHE is the particular heat exchanger selected for design for several reasons: 1) The working fluid mixture flows in both hot and cold sides, then the impact of transport properties estimate is enhanced; 2) a wide range of density conditions are encountered in the PCHE recuperator of the transcritical cycle, from high-pressure (HP) liquid to supercritical gas conditions; 3) few models are capable of describing with good accuracy and with continuity in the transcritical transition; 4) it represents the most cost-expensive component of the power block, then a reliable sizing is necessary; and 5) the recuperator effectiveness has great impact on the cycle efficiency, then an incorrect design would lead to inefficiencies.

Particular attention has been given to the selection of the most appropriate models to determine the heat transfer coefficient of the mixture. As a peculiarity of the transcritical cycles working with complex dopants is that partial condensation occurs near the recuperator cold-end, then there is a need to describe the mixture's behavior both in single-phase vapor and two-phase regions.

To date, PCHEs were experimentally and numerically studied with single-phase working fluids such as helium, water, and carbon dioxide; the results are well summarized in the work of Chai and Tassou.[12] Few efforts have been made in the two-phase field.[13] As regards mixtures, Kim et al.[14] investigated the thermal–hydraulic performance of PCHE experimentally and numerically with He/CO_2 mixture.

The PCHE recuperator has been sized with different transport properties models, starting from optimized power cycle conditions, for the CO_2 mixtures with hexafluorobenzene and decane: The TRAPP and Chung–Lee–Starling models were imported from Aspen Plus environment, since they are models applicable in a wide density domain, while the friction theory model was implemented (and calibrated) in an in-house MATLAB code.

Once the most appropriate methods are selected, the optimal PCHE design is carried out by minimizing the LCOE for a CSP field designed in Sevilla (Spain).

2. Transport Properties Models for CO_2 Mixtures

Viscosity is a physical property that measures the internal friction among fluid layers, and it is related to the rate of momentum diffusion due to existing velocity gradient. In the same way, thermal conductivity is correlated to the rate of heat flux resulting from a temperature gradient. Both viscosity and thermal conductivity are functions of temperature and pressure or density.

The starting point of the theoretical basis for the calculation of both viscosity and thermal conductivity at "zero-density"

conditions is the elementary kinetic theory of gases.[15] In this work, the Chung et al. model[16] is the kinetic-theory-based method selected for the evaluation of viscosity (Equation (1)) and thermal conductivity (Equation (4)) of the pure components. This method has been chosen because it is the most faithful to Chapman–Enskog theory, but also it employs the acentric factor (ω) and the dipole moment (μ) to account for the molecular shape, the polarity, and anisotropic intermolecular forces. In dilute-gas conditions, the mean expected deviation is lower than 1.5% for nonpolar gases and up to 4% for polar gases.[17] While rigorous theoretical methods are not suitable for the mixtures, so semi-empirical mixing rules has to be adopted. Wilke[18] proposed a semi-empirical formula for the evaluation of the binary mixture viscosity (Equation (2) and (3)), reporting an average deviation of less than 1% in comparison with experimental data of 17 mixtures.[18] Many methods have been proposed for the thermal conductivity of dilute-gas mixtures,[17] but the most commonly used is the empirical model proposed by Wassiljewa,[19] in Equation (5), where the function A_{ij} can be calculated as proposed by Mason and Saxena (Equation (6)).[20]

"zero-density" viscosity

$$\mu_{i,0} = 40.785 \frac{F_C (MT)^{\frac{1}{2}}}{V_C^{\frac{2}{3}} \Omega^{(2,2)}} \tag{1}$$

$$\mu_{m,0} = \sum_{i=1}^{n} \frac{\gamma_i \mu_{i,0}}{\sum_{j=1}^{n} \gamma_i \Phi_{ij}} \tag{2}$$

$$\Phi_{ij} = \frac{\left[1 + \left(\frac{\mu_i}{\mu_j}\right)^{\frac{1}{2}} \left(\frac{M_j}{M_i}\right)^{\frac{1}{4}}\right]^2}{\left[8 \left(1 + \frac{M_i}{M_j}\right)\right]^{\frac{1}{2}}} \tag{3}$$

"zero density" Thermal conductivity

$$\frac{\lambda_{i,0} M'}{\mu_{i,0} C_v} = \frac{3.75 \psi}{\frac{C_v}{R}} \tag{4}$$

$$\lambda_{m,0} = \sum_{i=1}^{n} \frac{\gamma_i \lambda_{i,0}}{\sum_{j=1}^{n} \gamma_j A_{ij}} \tag{5}$$

$$A_{ij} = \frac{\left[1 + \left(\frac{\lambda_{tr,i}}{\lambda_{tr,j}}\right)^{\frac{1}{2}} \left(\frac{M_i}{M_j}\right)^{\frac{1}{4}}\right]^2}{\left[8\left(1 + \frac{M_i}{M_j}\right)\right]^{\frac{1}{2}}} \tag{6}$$

While the transport properties models at low density have a solid theoretical basis, all methods practically used for dense gases and liquids are empirical or semi-theoretical.[17] In this scenario, the common approach considers the generic transport property π at high density as a sum of a "zero-density" term (π_0) and a pressure/density effect contribution $\Delta\pi(T,p)$ known as the "excess property" or "residual property".

$$\pi(T,p) = \pi_0(T) + \Delta\pi(T,p) \tag{7}$$

The zero-density term $\pi_0(T)$ is evaluated with the methods described previously, while each model distinguishes on how the residual term $\Delta\pi(T,p)$ is treated. The residual property can be defined with an empirical correlation, of density and temperature, regressed from experimental data, or it can be derived

from an extension of the kinetic theory (such as the extension of the Chung–Lee–Starling model for the viscosity of dense gases[21]).

The most successful approaches are based on the corresponding state principle. According to this principle, it is possible to evaluate the residual property of a pure fluid or mixture from the well-known available property of a reference fluid, which is evaluated in a corresponding state $(T_0, \rho_0) = \left(\frac{T}{f_i}, \rho h_i\right)$ with respect to a pure fluid "i" of interest. The scaling factors f_i and h_i, which are related to the ratios between the intermolecular potential function parameters (the depth of the potential well ϵ and the equilibrium distance σ), that are in turn proportional to the critical parameters (T_c, V_c) ratios from a macroscopic point of view. Thus

$$f_i = \frac{\epsilon_i}{\epsilon_{ref}} = \frac{T_{c,i}}{T_{c,ref}} \tag{8}$$

$$h_i = \frac{\sigma_i^3}{\sigma_{ref}^3} = \frac{V_{c,i}}{V_c^{ref}} \tag{9}$$

In case of mixtures, simple mixing rules are applied to the pure component factors for the calculation of the scaling factors f_m and h_m, considering that the properties of a mixture are consistent with the behavior of a hypothetical pure fluid which is conformal with the reference fluid. Since the straight application of the corresponding states is accurate only for similar molecules (said "conformal")[22] having similar intermolecular potential, Leach and co-workers[23] suggested the use of "shape factors" φ and θ to correct the reducing ratios, as described later. The authors suggested temperature-dependent correlations for the shape factors in terms of the Pitzer acentric factor and the critical compressibility factor.

$$f_i = \frac{T_{c,i}}{T_c^{ref}} \theta_i \tag{10}$$

$$h_i = \frac{V_{c,i}}{V_c^{ref}} \varnothing_i \tag{11}$$

The use of shape factors distinguishes the so-called "extended corresponding states" (ECS) methods. An example of an ECS method is the one used in the software Refprop[24] or in the method of Ely and Huber.[25] Exact shape factors can be obtained by solving the simultaneous equality of the residual dimensionless Helmholtz-free energy and the residual compressibility factors, then the resolution of a nonlinear system. Thus, Monnery[26] suggested to retrieve correlations for the shape factors directly from experimental data instead of thermodynamics.

Anyway, the one-fluid theory fails because the density effects are not well addressed when dealing with mixtures of components having high difference in size (especially for high molar volume ratios) since the real local composition of the mixture is different than the bulk, and it is dominated by the larger component.

The improvement on model reliability for these specific mixtures follows two paths: the use of a more "conformal" reference fluid, or another physically sound approach. In this work, CO_2 was adopted as reference fluid to improve the conformability

between the reference fluid and the CO_2-rich mixtures of interest in ECS methods. Moreover, the recent friction theory model[27] is investigated here. In the friction theory model, an EoS is used to compute the attractive and repulsive intermolecular interactions, in terms of attractive and repulsive pressure or entropy, that are used as input for the model to predict the transport property in a wide range of conditions. Since an EoS is capable of describing the interactions in a binary mixture in a wide range of thermodynamic conditions, it is a solid basis for a transport property model capable of describing even complex mixtures. In the following subsections, the most interesting models for dense CO_2 mixtures are discussed.

2.1. The TRAPP Method for Viscosity and Thermal Conductivity

The TRAPP (TRansport Property Prediction) method was presented by Ely and Hanley in 1981 as an extended corresponding states-based computer program for the prediction of viscosity and thermal conductivity in hydrocarbon mixtures[28] in both gas and liquid phases, using methane as reference fluid. Then, propane has been used in the more recent SUPERTRAPP model.[29] The residual property of the mixture $\Delta\eta_m$ is related to that of the reference fluid through appropriate mixing rules, as illustrated later.

$$\Delta\eta_m(T,\rho) = \eta_m(T,\rho) - \eta_m^0(T) = F_{\eta m}(\eta^R - \eta_0^R) + \Delta\eta_m^{ENSKOG} \tag{12}$$

$$F_{\eta m} = (M^R)^{-0.5}(h_m)^{-2}\sum_i\sum_j \gamma_i\gamma_j(f_{ij}M_{ij})^{0.5}(h_{ij})^{4/3} \tag{13}$$

where $\quad h_m = \sum_i\sum_j \gamma_i\gamma_j h_{ij} f_m h_m = \sum_i\sum_j \gamma_i\gamma_j f_{ij} h_{ij}$

In case of viscosity, an Enskog term $\Delta\eta^{ENSKOG}$[30] was introduced to improve the accuracy of the relation when the size difference of the two components in the binary mixture becomes large (absent for thermal conductivity). This is because the concentration of the larger component is locally higher than the bulk, and it controls the value of viscosity (since viscosity is dominated by short-range forces).

The "CO_2-SUPERTRAPP"[10] model has been also considered: The approach is the same as in the TRAPP method, but CO_2 is used as reference fluid with the polynomial correlation of Huber et al.[31] The CO_2-SUPERTRAPP model has not been used for the viscosity estimate since it does not provide a general improvement compared to the SUPERTRAPP model: the first overpredicts the property values while the latter typically underpredicts them, as stated by.[10]

2.2. The Pedersen and Christensen Model for Viscosity

The model of Pedersen and Christensen[22–24] (for viscosity evaluation lays its fundamentals on the work of Christensen (1980,[32]). The final formulation is

$$\mu_m(P,T) = \left(\frac{T_{C,mix}}{T_{C,0}}\right)^{-\frac{1}{6}}\left(\frac{P_{C,mix}}{P_{C,0}}\right)^{\frac{2}{3}}\left(\frac{M_{mix}}{M_0}\right)^{-\frac{1}{2}}\left(\frac{\alpha_{mix}}{\alpha_0}\right)\mu_0(T_0,P_0) \tag{14}$$

where the reference fluid, with the subscript "0", is evaluated at $T_0 = \frac{T}{\frac{T_{C,mix}}{T_{C,0}}\frac{\alpha_{mix}}{\alpha_0}}$ and $P_0 = \frac{P}{\frac{P_{C,mix}}{P_{C,0}}\frac{\alpha_{mix}}{\alpha_0}}$.

The α_{mix} and α_0 parameters are evaluated as

$$\alpha = 1 + 7.378 \cdot 10^{-3} \rho_R^{1.847} M^{0.5173} \tag{15}$$

The authors of this model suggest mixture's pseudo-critical parameters to be used, with simple mixing rules from the van der Waals one-fluid approximation. Although the reference fluid in the original model is methane, in this work carbon dioxide is chosen as reference fluid: the resulting so-called CO_2-Pedersen model has been used by Nazeri et al. (2016,[10]) for the estimation of CO_2 mixtures properties. An advantage of this model is that it does not require the density as input. However, high deviations are expected with complex compounds since mixture's critical properties are estimated with simple vdW mixing rules.

2.3. The Friction Theory Model for Viscosity

The friction theory model was developed by Quiñones-Cisneros et al.[27] implementing the residual viscosity term from a mechanical point of view. In analogy with the well-known Amontons–Coulomb friction law, the residual term (friction viscosity, η_f) is related to the attractive and repulsive pressure terms by means of friction coefficients, as described in Equation (16).

$$\eta = \eta_0 + \eta_f = \eta_0 + \sum_{i=1}^{n_a} k_{a,i} p_a^i + \sum_{i=1}^{n_r} k_{r,i} p_r^i \tag{16}$$

where $k_{r,i}$ and $k_{a,i}$ are the friction coefficient of the pure fluid, η_0 is the zero-density viscosity, and p_a^i and p_r^i are the ith order attractive and repulsive pressure deriving from an EoS.

At HP conditions, the intermolecular distance between the fluid layers decreases and the short-range intermolecular forces predominate over the long-range attractive forces. For this reason, a second-order truncation of the repulsive term ($n_r = 2$) is suggested, while a first-order truncation is sufficient for the attractive pressure term ($n_a = 1$).[33] Thus, the resulting quadratic equation of the friction theory model is shown in Equation (17).

$$\eta = \eta_0 + k_r p_r + k_a p_a + k_{rr} p_r^2 \tag{17}$$

In case of mixtures, the residual friction term is calculated in the same way, but mixing rules are applied for the mixture friction coefficients

$$k_j = \sum_i^n z_i k_{j,i} \quad \text{with} \quad j = a, r, rr \tag{18}$$

$$z_i = \frac{x_i}{M_i^\epsilon \cdot \sum_i \frac{x_i}{M_i^\epsilon}} \tag{19}$$

where $k_{r,i}$, $k_{a,i}$, and $k_{rr,i}$ are the friction coefficients of the n pure components in mixture having mole fraction x_i and molecular weight M_i; the exponent ϵ is typically assumed to be equal to 0.30.[27]

The pure fluid friction coefficients are obtained fitting the experimental residual viscosities: friction coefficients for many

alkanes, but also for carbon dioxide and nitrogen, can be found in the work of Quiñones-Cisneros and Deiters.[33] If friction coefficients cannot be retrieved due to the lack of experimental data for specific chemical compounds in a wide range of temperatures and pressures, the general corresponding states-based friction theory model can be used. In the general one-parameter friction theory model, the friction viscosity is expressed in a reduced form: the friction viscosity (residual) term η_f can be calculated from the reduced friction viscosity $\hat{\eta}_f$ and a characteristic critical viscosity η_c, which is the only one parameter of the model that has to characterized for each component in the mixture.

$$\hat{\eta}_f = \frac{\eta_f}{\eta_c} = \hat{\eta}_{f,r} + \hat{\eta}_{f,a} \tag{20}$$

By adopting the general one-parameter model, the reduced friction viscosity $\hat{\eta}_f$ is calculated in the same way as in Equation (16), but with the pure-component friction factors $k_{j,i}$ described as

$$k_{j,i} = \frac{\eta_{c,i} \, \hat{k}_{j,i}}{P_{c,i}} \tag{21}$$

$$\hat{k}_{j,i} = \hat{k}_{j,c} + \Delta \hat{k}_{j,i} \tag{22}$$

where the critical isotherm contribution, with the subscript "c", depends on the selected EoS, while the residual temperature-dependent contribution depends also on the pure-component critical temperature.

The characteristic critical viscosity of the pure compounds $\eta_{c,i}$ is the only real degree of freedom of the model, resulting in the choice of the cubic EoS: in this work, the PR and SRK EoS have been evaluated for this purpose. As the results provided from these cubic EoS are very similar, the PR-EoS, and the corresponding model, is then called f-PR model.

2.4. The Friction Theory Model for Thermal Conductivity

Whereas the friction theory model for viscosity has a direct derivation from mechanical considerations on the shear stress among fluid layers, the relationship between thermal conductivity and thermodynamic caloric properties is not as intuitive. In similarity with the f-theory model for viscosity (Equation (16)), Quiñones-Cisneros et al.[34] developed the friction theory model as follows

$$\lambda = \lambda_0 + \lambda_f + \lambda_c = \lambda_0 + \sum_{i=1}^{n_a} \varphi_{a,i} s_a^i + \sum_{i=1}^{n_r} \varphi_{r,i} s_r^i + \lambda_c \tag{23}$$

where $\varphi_{r,i}$ and $\varphi_{a,i}$ are the friction coefficients of the pure fluid, η_0 is the zero-density viscosity, s_a^i and s_r^i are the ith order attractive and repulsive residual entropy terms, which can be derived from an EoS. The critical enhancement term is reported to be

$$\lambda_c = \varphi_c \rho^3 \Big/ \left(\frac{\partial p}{\partial v}\right)_T \tag{24}$$

The authors suggested a second-order truncation, so the formulation can be made explicit as

$$\lambda = \lambda_0 + \lambda_c + \varphi_{a,1} s_a + \varphi_{a,2} s_a^2 + \varphi_{r,1} s_r + \varphi_{r,2} s_r^2 \tag{25}$$

The friction coefficients can be defined with the following expressions

$$\varphi_{a,1} = a_0 \exp\left[a_1\left(\frac{T_c}{T} - 1\right) + a_2\left(\left(\frac{T_c}{T}\right)^2 - 1\right)\right] \tag{26}$$

$$\varphi_{r,1} = b_0 \exp\left[b_1\left(\frac{T_c}{T} - 1\right) + b_2\left(\left(\frac{T_c}{T}\right)^2 - 1\right)\right] \tag{27}$$

$$\varphi_{a,2} = A_0 \tag{28}$$

$$\varphi_{r,2} = B_0 \tag{29}$$

Thus, nine coefficients (a_i, b_i, A_0, B_0, φ_c) need to be regressed for each chemical species using experimental thermal conductivity data of the pure fluid. Friction coefficients are already available in ref. [34] for many compounds including CO_2 and some hydrocarbons. In this work, the PR-EoS is used to obtain the residual attractive and repulsive entropy terms.

In case of mixtures, simple mass fraction-based mixing rules are applied to the friction coefficients as suggested by Quiñones-Cisneros. The validation of the model for mixtures is still an open point due to very few reliable experimental data are available. For this reason, a general one-parameter f-theory model for thermal conductivity is still missing. However, the model is reported to be satisfactory for most of the mixtures evaluated.[34]

3. Transport Properties Models Validation with CO$_2$ Mixtures Experimental Data

The transport properties models described in the previous section were implemented in MATLAB environment[35] for their validation with proper CO_2 mixtures experimental data. A survey of available CO_2 mixtures experimental data was carried out. Looking at the application in transcritical cycle, particular attention was given to dataset in the dense region (high operating pressure) and to mixtures with heavy and complex dopants. The few experimental data available for CO_2 mixtures mainly come from the CCS sector where most of them concern the gas field at room pressure.[9] The selected pure fluids are N_2 and some lightweight (CH_4, C_2H_6) and heavy hydrocarbons ($C_{10}H_{22}$, $C_{12}H_{26}$). Their molecular parameters are reported in **Table 1** together with the values of pure CO_2. Although the main investigated dopant is a perfluorocarbon, the n-decane can be used as a reference fluid for the transport properties validation

Table 1. Main characteristics of pure components.

Species	MW [kg kmol^{-1}]	P_C [bar]	T_C [K]	V_C [cm^3 mol^{-1}]
CO$_2$	44.010	74.74	304.12	94.07
N$_2$	28.010	33.98	126.20	90.10
CH$_4$	16.043	45.99	190.56	98.6
C$_2$H$_6$	30.07	48.72	305.32	145.5
C$_{10}$H$_{22}$	142.285	21.10	617.70	624
C$_{12}$H$_{26}$	170.338	18.20	658.00	754

Table 2. Viscosity models comparison with experimental data.

Mixtures	Phase	References	NP	T [K]	P [bar]	AAD [%]		
						f-theory	SUPERTRAPP	CO_2-Pedersen
$CO_2 + N_2$	G	[67]	35	293	1–22	2.57	2.45	0.6
$CO_2 + CH_4$	G	[68]	88	323–473	3.3–69.7	4.58	4.55	2.77
$CO_2 + C_2H_6$	G-L	[69]	70	280–320	21–348	7.12	9.4	/
$CO_2 + C_{10}H_{22}$	L	[70]	70	311–403	69–347	7.1	17.3	/
$CO_2 + C_{12}H_{26}$	L	[36]	20	284–351	14–142	9.9	24.2	/

due to its molecular mass and complexity. The comparison with the data available in the gas phase at ambient pressure was excluded because they are outside the range of interest and typically the zero-density properties models are particularly accurate (with an average error typically below 3–4%[17]). The models accuracy is represented by the percentage average absolute deviation (AAD%), between the calculated and the experimental values weighted on the number of available data (see Equation (30)). **Table 2** reports the AAD% of the models in comparison with the experimental viscosity in gas or liquid phase at various molar compositions.

$$AAD\% = \sum_i \frac{|\eta_i - \eta_{i,\text{exp}}|}{N_{\text{points}}} \cdot 100 \qquad (30)$$

As stated by Nazeri et al.,[10] the CO_2-Pedersen represents the best model of viscosity for CO_2 mixtures in CCS application, i.e., with lightweight and simple compounds. However, since the methods implement simple mixing rules for the mixture's critical parameters, it is not reliable with complex mixtures and for this reason its results are reported only for two datasets in Table 2.

Even if the TRAPP method is extendable into the liquid region, the density effects are very much influenced by mass and molecular size differences between the reference fluid (propane in the SUPERTRAPP) and the component in the binary mixture. These discrepancies are more evident when the critical volume of the component increases compared to the critical volume of the reference fluid, which is representative of high size differences

$$\left(\frac{\sigma_i}{\sigma_0}\right)^3 \cong \frac{\rho_o^c}{\rho_i^c} = \frac{V_o^c}{V_i^c} \qquad (31)$$

The local size differences especially affect the viscosity estimation considering that, at high densities, the momentum transport takes place predominantly by intermolecular forces rather than collisions between molecules in free flight. A second-order effect of the repulsive intermolecular forces is considered into the friction theory model for viscosity, making it physically consistent.

As it can be noted, when the complexity of the mixture increases, the one-fluid theory lead to high errors (more than 15%). **Figure 1** shows, as an example, the comparison between the experimental viscosities of the CO_2/n-dodecane mixture and the estimated values. This particular dataset has also been evaluated in the literature with specific models for liquids based on the
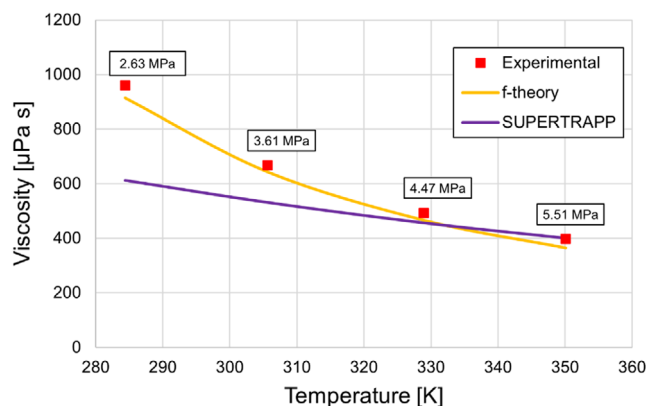

Figure 1. Experimental and calculated viscosities comparison for 40% CO_2 + n-dodecane mixture at different temperature and pressure.

Eyring theory,[36] but without success: the reported AAD of the Grunberg and Nissan model was 63%, while the Katti and Chaudri model achieves an AAD equal to 43%. So it is possible to conclude that the friction theory model has the largest potential of providing accurate estimate when dealing with complex and dense mixtures.

As regards the thermal conductivity, the comparison between the scarce experimental data from the literature and the considered models is illustrated in **Table 3**. The recent data of Patek et al.[37] have been selected for the comparison of the $CO_2 + CH_4$ mixture in the gas phase, while the recent data of Kim et al.[38] have been used for the dense-liquid phase.

An improvement in the thermal conductivity prediction can be noted when carbon dioxide is used as reference fluid (CO_2-SUPERTRAPP) with respect to propane. However, regarding the CO_2 + n-decane mixture, the comparison with the data in ref. [39] shows how the corresponding states-based models fail when dealing with complex mixture, especially in the dense-liquid phase. Instead, the adoption of the friction theory model, with optimized friction coefficients (as explained in the following section), yields reasonably good results with an AAD of about 4%.

This preliminary analysis confirms that the f-theory has the largest potential of providing reliable results even for asymmetric mixtures in a wide range of operating conditions, thus it will be used to estimate the transport properties for the PCHE recuperator design of the two case studies.

Table 3. Thermal conductivities models comparison with experimental data.

Mixtures	Phase	References	NP	T [K]	P [bar]	AAD %		
						f-theory	SUPER TRAPP	CO_2-SUPER TRAPP
$CO_2 + CH_4$	G	[37]	180	300–425	7.27–119.7	3.13	8.66	1.34
$CO_2 + CH_4$	L	[38]	8	223.7–295.6	71.4–198.5	5.16	5.17	5.01
$CO_2 + N_2$	L-SC	[38]	11	223.8–308.4	54.5–201.5	4.72	5.05	5.68
$CO_2 + N_2$	G	[71]	22	321.4–381.8	11–250	1.74	9.84	2.2
$CO_2 + N_2O$	G	[72]	33	300.65	8–42.5	1.2	1.3	2.28
$CO_2 + C_{10}H_{22}$	L	[39]	23	298.15–328.15	11.3–105	4.03	21.1	22.3

4. Friction Theory Models Optimization for the Case Studies

The friction theory models for viscosity and thermal conductivity are optimized here for the two selected CO_2 blends, $CO_2 + C_{10}H_{22}$ and $CO_2 + C_6F_6$. The model predictions are compared with two models identified in Aspen Plus environment,[40] valid in both gas and liquid fields: the Chung–Lee–Starling and TRAPP methods. The friction theory models are fitted with selected experimental data of the pure components of the mixture. Data in dense conditions are crucial for a proper characterization of the residual property (friction term). About the critical characteristic viscosity of the pure compound compounds $\eta_{c,i}$, only one parameter has to be fitted. On the other hand, nine coefficients (a_i, b_i, A_0, B_0, φ_c) need to be regressed in the friction theory model for thermal conductivity. The regression is carried out in MATLAB environment by using a nonlinear least-squares optimization with Levenberg–Marquardt algorithm. The results of the fitting procedure are presented in **Table 4**.

4.1. $CO_2 + $ n-Decane Mixture: Viscosity and Thermal Conductivity Assessment

For the reference mixture, the general one-parameter f-theory model for viscosity (Equation (16)–(22)) is available in literature with the characteristic critical viscosities optimized both for CO_2[41] and n-decane[27]: $\eta_{c,CO2} = 376.872\,\mu P$ and $\eta_{c,C10H22} = 257.928\,\mu P$. As already presented in Table 2, these coefficients allow the estimation of the viscosity with reasonably good results (with an AAD of 7%). As an example, **Figure 2** shows the calculated viscosities with the three models compared with liquid experimental measurements at 311 K and a CO_2 molar content of 15%. The TRAPP and the Chung–Lee–Starling models are far from the real mixture behavior, overestimating and underestimating the experimental dynamic viscosities respectively with a minimum AAD of 19%.
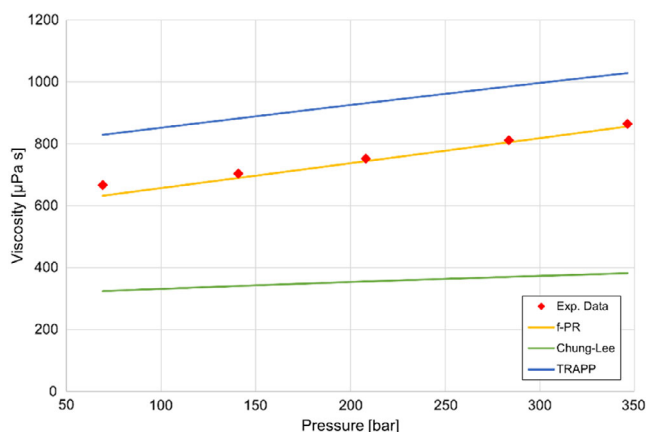

Figure 2. Comparison among viscosity models, 15%CO_2 + n-decane mixture ($T = 311$ K).

The thermal conductivity of the mixture has been modeled with the friction theory model for thermal conductivity (Equation (23)–(29)). The nine coefficients, reported in Table 4, of the pure CO_2 are taken from the original model.[34] On the other hand, the friction coefficients of pure n-decane, proposed in ref. [34], lead to large deviations when they are adopted for the mixture, even if the agreement with pure n-decane experimental data was very good. For this reason, the parameters of the pure n-decane were here regressed against the recent experimental data of Zheng et al.[42] providing an AAD = 0.87%. To obtain f-theory coefficients that provide good results also for the mixture, some constraints have been imposed in the regression to have sign concordance of the coefficients (A_0, B_0) of both n-decane and CO_2 associated to the quadratic residual entropy. As reported in Table 3, the f-PR model with the coefficients in Table 4 has an AAD equal to 4.03%, while the corresponding states models have deviations over 15%. In **Figure 3**, some experimental thermal conductivities at different mixture
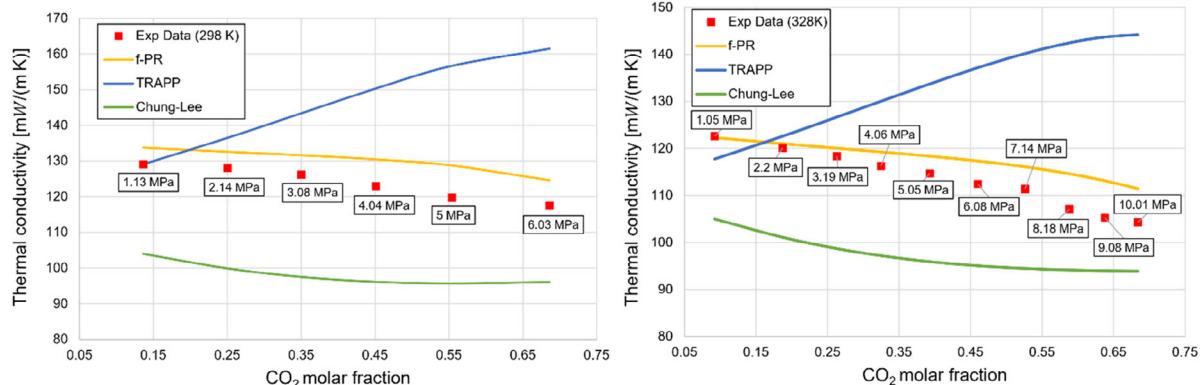
Table 4. Optimized parameters for the friction coefficients of the f-theory thermal conductivity model.

	a_0	a_1	a_2	b_0	b_1	b_2	A_0	B_0	Φ_c
CO_2	−0.3868	35.6309	−15.9827	−3.6295	2.6629	−2.6629	0.2274	0.3120	−0.6579
$C_{10}H_{22}$	0.0330	11.6087	−2.6466	−1.5481	20.00	−10.3860	0.0616	0.0171	−0.0072
C_6F_6	−0.9287	5.5583	−1.8031	−0.0344	0.0022	0	0.0142	0.0018	−0.0408

Figure 3. Comparison between models and experimental data (298 K left, 328 K right) of CO_2 + n-decane.

compositions[39] are compared with the calculated values with the three models. The measurements are characterized by two different temperatures (298 and 328 K) and a pressure range of 1–10 MPa. Results agree with the viscosity outcome: the TRAPP model overestimates the thermal conductivity of the mixture especially at high carbon dioxide fractions (AAD = 18.4%), while the Chung–Lee model gives the opposite trend with a similar AAD (17.1%).

4.2. $CO_2 + C_6F_6$ Mixture: Viscosity and Thermal Conductivity Assessment

To calibrate the general one-parameter f-theory model for viscosity in case of pure C_6F_6, the relatively recent experimental liquid viscosities of Freire et al.[43] have been mainly used. As mentioned by Freire et al., viscosity measurements of fluorocarbons in literature are scarce and often discordant. Moreover, the viscosity of fluorinated compounds is remarkably higher than their homologous hydrocarbons[43]; and the viscosity increases from linear structures to cyclic and aromatic structures (i.e., C_6F_6). Even if only five data points are available for the C_6F_6 in the temperature range 298.15–318.15 K, they are crucial to assess the behavior of its viscosity at high densities (liquid-phase region) and then to characterize the residual term. Some experimental data of Dymond et al.[44] are also used for a better regression at

higher temperature (up to 323.2 K) and pressure (0.1–47.7 MPa). Some data are excluded from the evaluation since there are some inconsistences: for example, at atmospheric pressure, there are liquid viscosities data above the normal boiling temperature. The regressed value of critical characteristic viscosity is $\eta_{c, C6F6} = 640.76\,\mu P$, which guarantee a mean absolute deviation of 6.1% that is satisfactory for the scope of this work, as can be seen in **Figure 4** (left). Results of the TRAPP and Chung–Lee–Starling models, in Figure 4 (right), show large deviations from the experimental data.

The f-theory model for thermal conductivity has been optimized by regressing the friction coefficients on the only three liquid data at ambient pressure available for C_6F_6 from Irving et al.[45] Additional data obtained by the interpolation of the Irving experimental data were needed to find the nine friction coefficients. For a better fitting procedure, more experimental points would be necessary. However, even few data in the liquid phase are helpful in the characterization of the residual friction term since the residual attractive and repulsive entropies are high in the liquid phase. The regressed parameters that describe the friction coefficients are reported in Equation (23)–(29). In conclusion, the resulting mixture behavior in terms of transport properties cannot be validated because no experimental measurements has been found in literature for this specific dopant. The comparison of the models with the experimental data, in
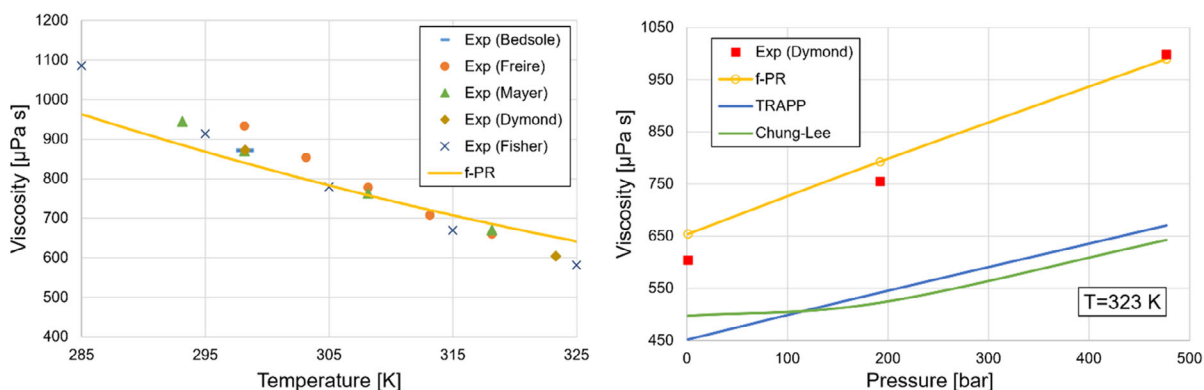

Figure 4. f-PR vs experimental liquid viscosity of pure C_6F_6 at ambient pressure (left); comparison with isothermal data at high pressure (right).
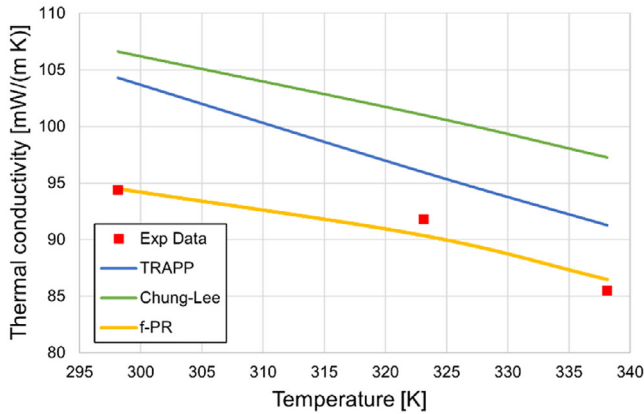
ADVANCED
SCIENCE NEWS
www.advancedsciencenews.com

Energy Technology
Generation, Conversion, Storage, Distribution
www.entechnol.de

Figure 5. Liquid thermal conductivity of pure C_6F_6 at ambient pressure (Irving et al.) vs models.

Figure 5, shows that the results of the TRAPP and Chung–Lee models overestimate the measurements.

As reported by Irving, the thermal conductivity of fluorinated hydrocarbons is lower than that of the corresponding hydrocarbons. The more the fluorine atoms in the molecule, the lesser is the thermal conductivity if compared to the same hydrocarbon structure. As it can be noted, in fact, the thermal conductivity of pure C_6F_6 is relatively low considering that it is in the liquid phase at medium-low reduced temperatures (0.56–0.65), where the density is very high (1614 kg m^{-3} at 298 K and 1 atm according to Counsell et al.[46]) if compared to benzene whose thermal conductivity is about 150% higher in the same conditions.

In conclusion, the resulting mixture behavior in terms of transport properties cannot be validated because no experimental measurements has been found in literature for this specific dopant.

5. PCHE Recuperator Design Methodology

The transport properties are implemented into a PCHE design code to define the heat transfer coefficients and its size. PCHEs are composed by an alternation of overlapping hot and cold plates (in which minichannels are chemically etched) that are joined by means of a diffusion bonding process. A stack of plates (**Figure 6**) is jointed to form a core block of the desired geometry, called unit. The total PCHE volume consists of blocks with dimensions up to $0.6 \times 0.6 \times 1.5$ m. If larger heat exchangers are required, multiple blocks can be welded together. The width L_x of a single plate is limited to 0.6 m, and a stack of plates L_y equal to 0.6 m is usually used in the diffusion bonding procedure, while the maximum axial length of the block is fixed by the maximum plate length of 1.5 m.[47] In this work, the most applied configuration with counter-current flow in 2 mm width straight minichannels is considered with channel pass equal to 2.4 mm and a plate thickness t_p equal to 1.5 mm. The mechanical integrity of the PCHE with the considered channel geometry is verified as in ref. [48].

A segment-by-segment method is implemented to catch the local variations of the mixture thermophysical properties. The PCHE recuperator has been discretized along the axial direction into N segments (subheat exchangers), as shown in **Figure 7**, characterized by the same exchanged thermal duty, following the approach proposed by Jiang et al.[49]

The thermophysical properties of the mixture are calculated locally at the segment temperature and at its pressure level (considering the pressure drop in the segment). The axial length $L_{z,i}$ of the PCHE segment is evaluated with logarithmic mean temperature difference method once the local convective heat transfer coefficients of both sides $h_{hot,i}$ and $h_{cold,i}$ are estimated with appropriate models. Convergency is reached on the free-flow area to guarantee the design with desired % pressure drop in the LP side.
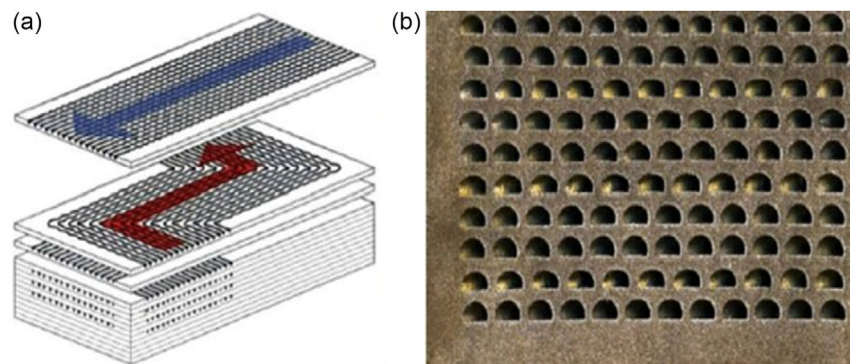

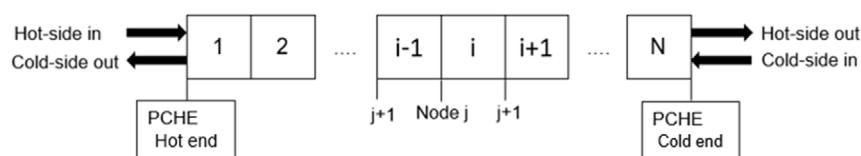**Figure 6.** PCHE: a) Plate stack, b) module cross section.[66]

Figure 7. Segmentation procedure adopted for the PCHE design.

ADVANCED
SCIENCE NEWS
www.advancedsciencenews.com

Energy Technology
Generation, Conversion, Storage, Distribution
www.entechnol.de

The number of channels per plate $N_{ch,P}$ and the number of plates N_P in a block are obtained from Equation (32) and (33), respectively. Each block has side margins (depending on header thickness and the attachment welds) and block ends that do not accommodate channels; a side margin $\Delta\delta$ of 50 mm and end plates $\Delta\gamma$ of 5 mm are assumed here.

$$N_{ch,P} = int\left(\frac{L_x - 2 \cdot \Delta\delta}{pass}\right) \tag{32}$$

$$N_P = int\left(\frac{L_y - 2 \cdot \Delta\gamma}{t_p}\right) \tag{33}$$

The recuperator is made by SS316 since it is compatible with the operating conditions of interest.[50] The metal thermal conductivity is considered as in ref. [51], and the roughness of the channel is assumed to be 10 μm. Dewson and Gray reported a cost of 30 \$ kg^{-1} in 2003[52] based on the weight of the delivered SS316-based PCHE. The cost per kg is actualized by using the medium Chemical Engineering Plant Cost Index of the period January–April 2022.[53] The final value is then 66 \$ kg^{-1}. Thus, the recuperator capital cost is estimated as

$$PCHE_{cost} = (V - V_{channels})\rho_{SS316}\, C_{SS316} \tag{34}$$

$$V_{channels} = A_{ch}\, N_{ch,tot}\, L_z \tag{35}$$

where ρ_{SS316} is equal to 7980 kg m^{-3}. This correlation comes from commercial practice for the cost evaluation based on the real PCHE weight, subtracting the volume occupied by channels.[54]

For the calculation of the local (each segment) heat transfer coefficients and pressure drop, models valid for both single-phase and two-phase flow are considered as partial condensation occurs in the LP side. The heat transfer coefficient has been computed with accurately selected models in both single-phase region and two-phase region, since partial condensation occurs inside the PCHE recuperator for the CO$_2$-based mixtures considered. The Gnielinski correlation can provide a good match between simulated and experimental results in case of straight

channels PCHE, as in this work, with a maximum error of 5%.[55] Moreover, as there are no experimental works on two-phase flows in PCHEs, we adopted a heat transfer coefficient model for two-phase mixtures that we have validated in a previous experimental work on a CO$_2$ mixture.[56] The correlations are discussed in detail in the Supporting Information section.

6. Power Cycle Application: PCHE Design and Impact

The assessment of the two CO$_2$-based power cycles applied in CSP context is carried out to show the impact of the transport properties prediction on the design of the PCHE recuperator as well as on the cycle performance. The mixture with n-decane is here considered as a reference CO$_2$ blend with heavy compounds due to the well-known thermo-physical mixture properties. The cycle results and the thermodynamic input parameters for the PCHE design are obtained in the Aspen Plus. The simple recuperative cycle layout and its representation in the T-s diagram are reported in **Figure 8**. In this configuration, the fluid is typically in the two-phase region at the outlet of the recuperator LP side (6). The condensation of the mixture is completed in the condenser (6-1). The design of the PCHE has been carried out starting from a base case of 1% pressure drop across the LP side ($\Delta P_{H,rec}$), and then increasing the values (up to 4%) to highlight the impact of the design on the capital costs and the cycle performance.

The main assumptions of the power cycles are summarized in **Table 5**: most of the values are taken from previous studies.[8,57–59] The maximum temperature depends on the mixture thermal stability and, as a consequence, on the related CSP technology: for the CO$_2$ + C$_6$F$_6$ mixture, the power cycle can be coupled with a CSP-tower plant configuration with molten salts as HTF, while, for the CO$_2$ + C$_{10}$H$_{22}$ mixture, a linear Fresnel reflector with commercial HTFs is considered. However, long-term thermal stability of the latter should be investigated: the selected temperature level (350 °C) is in line with the upper limit range for thermal stability of hydrocarbons and n-Decane experimental data availability range (up to 402 °C).

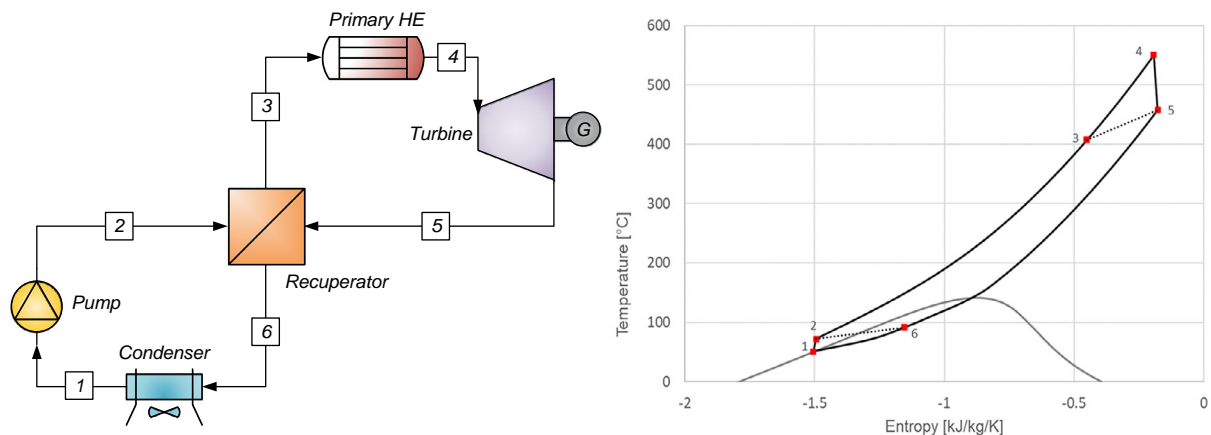**Figure 8.** Plant layout of the cycle working with CO$_2$ mixtures (left). T-s diagrams of transcritical CO$_2$ + C$_6$F$_6$ mixture with $x_{CO_2} = 84\%$ molar (right); the regeneration is highlighted by dashed lines.

Table 5. Assumptions for the power cycle simulations.

Parameters	Units	$CO_2 + C_{10}H_{22}$	$CO_2 + C_6F_6$
		Values	Values
$T_{min,cycle}$	°C	51	
$T_{in,turb}$	°C	350	550
$P_{in,turb}$	bar	250	
$\Delta T_{min,rec}$	°C	5	
$\Delta P_{H,rec}$	% [bar]	1 (1.1)	1 (0.81)
$\Delta P_{C,rec}$	bar	0.45a)	0.23a
ΔP_{PHE}	%	2	
ΔP_{COND}	%	2	
Turbine/Pump Isentropic Efficiency	%	92/88	

a)The pressure drop in the HP side is in accordance with the design results.

The composition of the mixture is optimized to achieve the maximum cycle efficiency at the selected operating conditions. The evaluation of the power cycle performance at the various PCHE design will include the cycle thermodynamic efficiency and the effectiveness of the recuperator, defined in Equation (36) and (37), respectively.

$$\eta_{Cycle} = \frac{W_{Turbine} - W_{Pump}}{Q_{in}} \qquad (36)$$

$$\epsilon_{Rec} = \frac{Q_{Recuperated}}{Q_\infty} = \frac{h(T_3, P_3) - h(T_2, P_2)}{h(T_5, P_5) - h(T_2, P_6)} \qquad (37)$$

A detailed description of the results of the recuperator can be found in the section of the $CO_2 + C_6F_6$ mixture, while the section of the $CO_2 + C_{10}H_{22}$ mixture is aimed to highlight the relevance of the properties estimation for a mixture with accessible experimental data on transport properties.

6.1. CO_2 + n-Decane Mixture

The power cycle is evaluated for a net power output of 50 MW. The PR EoS with an optimized binary interaction parameter $k_{ij} = 0.1141$[60] is used. From a preliminary analysis, the mixture
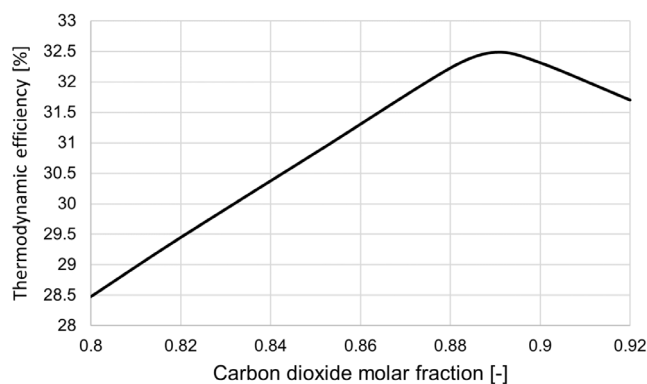
composition that maximize the cycle efficiency corresponds to a CO_2 molar fraction of 89%, as shown in **Figure 9**. **Table 6** collects the main operating conditions of the cycle for this composition, while the cycle power balance and the main PCHE features at design condition (base case with 1% $\Delta P_{H,rec}$) are reported in **Table 7**. It can be noticed that the amount of recovered heat power in the recuperator is remarkably high for this working fluid, if compared to the net mechanical power and the thermal power input. The T-Q diagram of the PCHE recuperator is shown in **Figure 10**. The minimum internal temperature approach (5 °C) is encountered at 28% of the total exchanged thermal duty

Table 6. Mixture $CO_2 + C_{10}H_{22}$: main thermodynamic conditions (base case 1% $\Delta P_{H,rec}$).

Streams	T [°C]	P [bar]	x_{vap} [-]
1	51	106.3	0
2	68.2	255.6	0
3	282.4	255.1	1
4	350	253	1
5	294.9	109.5	1
6	75.9	108.4	0.6

Table 7. Mixture $CO_2 + C_{10}H_{22}$: cycle performance at design conditions (base case 1% $\Delta P_{H,rec}$).

Parameter	units	Value
$\dot{m}$	kg s^{-1}	1200.7
W_{pump}	MW	28.7
Q_{rec}	MW	516.9
Q_{PHE}	MW	154.1
W_{turb}	MW	78.7
Q_{cond}	MW	104.1
UA_{rec}	MW K^{-1}	70.7
ϵ_{rec}	%	96.2
η_{cycle}	%	32.5

Figure 9. Mixture $CO_2 + C_{10}H_{22}$: cycle thermodynamic efficiency as a function of the mixture composition.
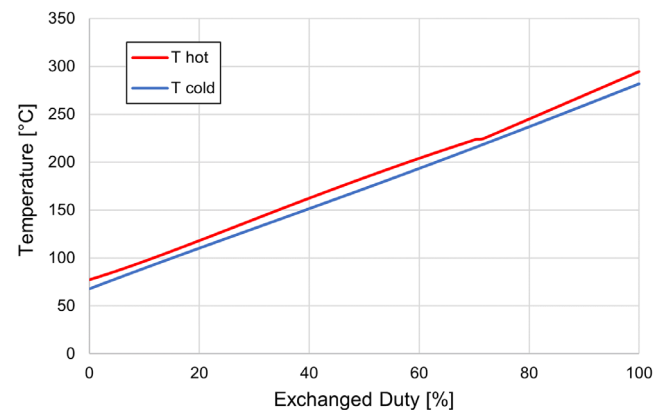
Figure 10. Mixture $CO_2 + C_{10}H_{22}$: T-Q diagram of the recuperator (base case 1% $\Delta P_{H,rec}$).

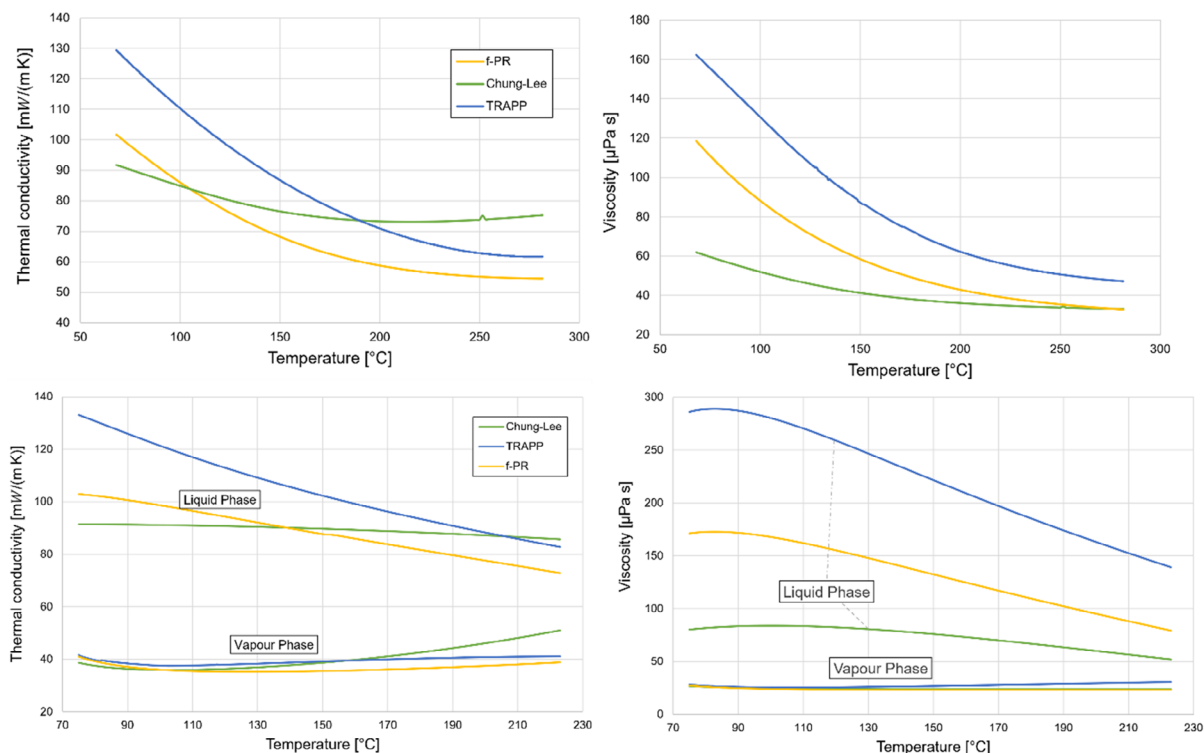**Figure 11.** Mixture $CO_2 + C_{10}H_{22}$: thermal conductivity and viscosity calculated with different models in the HP side (top) and in the two-phase region LP side (bottom) of the recuperator.

near the recuperator hot-end, where the dew point occurs (around 224 °C), thus the heat transfer mostly falls in the two-phase region for the hot side. The well-balanced heat capacities of the two streams inside the recuperator yield a good thermodynamic efficiency of the cycle although the turbine inlet temperature is 350 °C.

The design of the PCHE recuperator is carried out with three different models for the prediction of the transport properties: the TRAPP model, the Chung–Lee–Starling model, and the friction theory model (f-PR). The trend of the dynamic viscosity and thermal conductivity of the mixture at the upper and lower (two-phase field) isobars in the heat exchanger temperature range

is represented in **Figure 11**. The differences between the models are quite evident, especially at low temperatures in the HP side and in the liquid phase at LP. On the other hand, the values of the

Table 8. Mixture $CO_2 + C_{10}H_{22}$: PCHE design results (base case 1% $\Delta P_{H,rec}$) with different transport properties models.

	TRAPP	f-PR	Chung-Lee
G [kg sm^{-2}]	403	396	428
$N_{ch,hot/cold} \times 10^6$	1.897	1.93	1.79
L_z [m]	8.36	7.95	7.22
A [m^2]	81 523	78 904	66 301
V [m^3]	164.8	159.5	134
Cost [M\$]	60.6	58.6	49.2

Table 9. Mixture $CO_2 + C_6F_6$: main thermodynamic conditions (base case 1% $\Delta P_{H,rec}$).

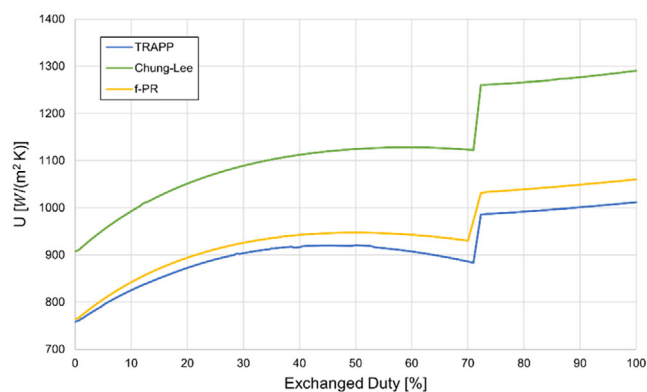| Streams	T [°C]	P [bar]	x_{vap} [-]
1	51	77.7	0
2	71.9	255.5	0
3	406	255.1	1
4	550	250	1
5	457.5	80.1	1
6	90.1	79.3	0.53

Figure 12. Mixture $CO_2 + C_{10}H_{22}$: U along the PCHE for $CO_2 + n$-decane, model comparison (base case 1% $\Delta P_{H,rec}$).

ADVANCED
SCIENCE NEWS
www.advancedsciencenews.com

Energy Technology
Generation, Conversion, Storage, Distribution
www.entechnol.de

vapor phase at LP are quite in agreement. It is evident that the TRAPP model results are higher with respect to those of the f-PR model: this is in accordance with the experimental data comparison shown in Figure 2.

The trend of the overall heat transfer coefficient U along the heat exchanger is illustrated in **Figure 12**. It is possible to conclude that the heat transfer area obtained with TRAPP and friction theory models are similar even if the transport properties are differen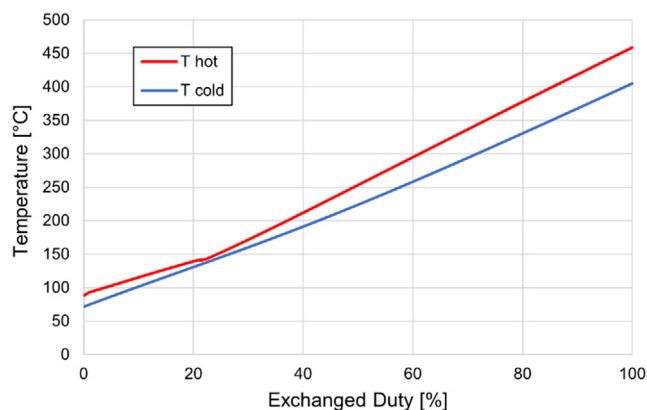tly predicted: an overestimation of the viscosity by the TRAPP model leads to lower Reynolds and Nusselt numbers, but this is compensated by an overestimation of the thermal conductivity in the calculation of the heat transfer coefficient.

The results of the design using the different models are reported in **Table 8**. Since the Chung–Lee–Starling method seems to underestimate the viscosity of this mixture (as proved by the experimental comparison in Figure 2) without penalizing the thermal conductivity, the high Reynolds numbers favor the heat transfer, and the heat exchanger results are more compact.

6.2. $CO_2 + C_6F_6$ Mixture

The power cycle is evaluated for a net mechanical power output of 100 MW and properties assessment is carried out with the PR EoS, by using an optimized BIP from.[6] A mixture composition with a CO_2 molar content of 84% is chosen according to the same work[6] to maximize the gross cycle efficiency (around 42%). The most relevant thermodynamic points of the cycle are summarized in **Table 9** for the base case. To see the impact of the PCHE design on the cycle performance, the hot-side pressure drops have been varied from 1 to 4% (corresponding to $0.81 \div 3.2$ bar). The cycle power balance and the main PCHE features at design condition are reported in Table 11.

The T-Q diagram of the PCHE recuperator is shown in **Figure 13**, where the internal pinch point is identified at the dew point near the cold-end. The values of the dynamic viscosity
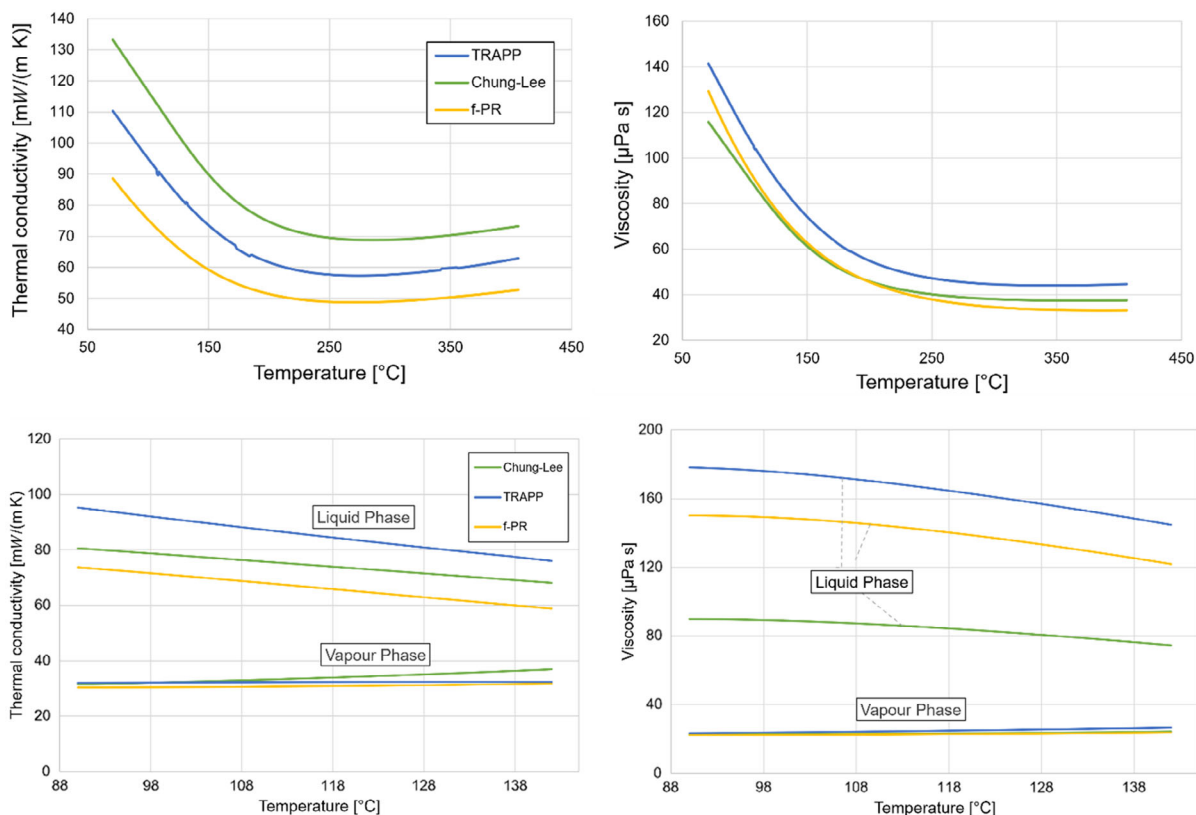

Figure 13. Mixture $CO_2 + C_6F_6$: T-Q diagram of the PCHE (base case 1% $\Delta P_{H,rec}$).

Figure 14. Mixture $CO_2 + C_6F_6$: thermal conductivity and viscosity calculated with different models in the HP side (top) and in LP side two-phase region (bottom) of the recuperator in the heat exchanger temperature range.
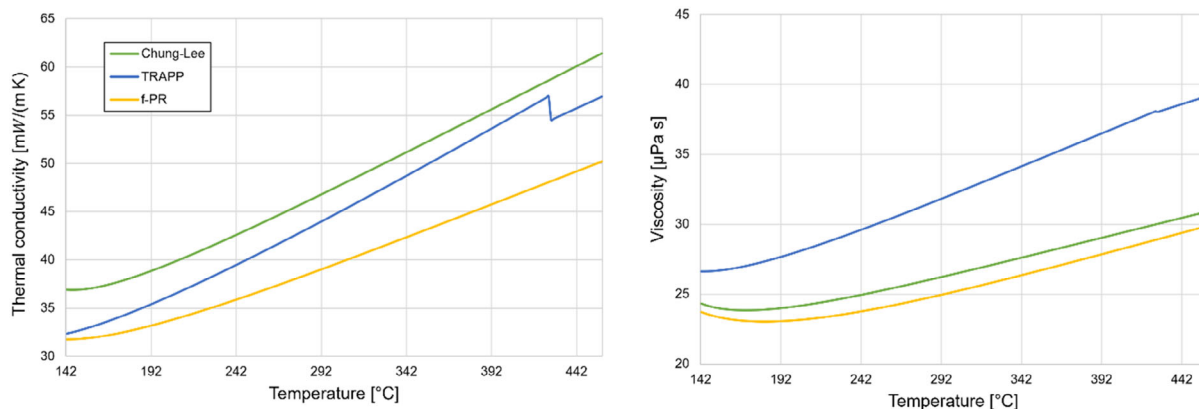
ADVANCED
SCIENCE NEWS
www.advancedsciencenews.com

Energy Technology
Generation, Conversion, Storage, Distribution
www.entechnol.de

Figure 15. Mixture $CO_2 + C_6F_6$: transport properties in the single-phase LP side with different models.

and thermal conductivity of the mixture along the upper and lower (two-phase field) isobars in the heat exchanger temperature range, calculated with the three investigated transport properties models, are represented in **Figure 14**. Moreover, **Figure 15** shows the same properties in the single-phase LP side of the recuperator.

It can be noted that the thermal conductivity predicted with the f-PR model is lower if compared to the other two models as shown in Figure 5 where both TRAPP and Chung–Lee models overestimate the experimental data of pure C_6F_6. The overall heat transfer coefficient is reported in **Figure 16**. In the HP stream, the viscosity increases about four times from the hot-end to the cold-end: this enhancement across critical conditions entails a drastic variation of the Reynolds number. Consequently, there is a reduction of the convective heat exchange performance at the cold-end that is only partially relieved by the increase of the thermal conductivity in that region. The counterbalanced trends of viscosity and thermal conductivity in the cold-side are well represented by the Prandtl numbers and the Reynolds number in **Figure 17**.

In the LP stream, the Reynolds number increases due to a reduction of the viscosity between the hot-end and the condensation onset, thus enhancing even the Nusselt number. However,
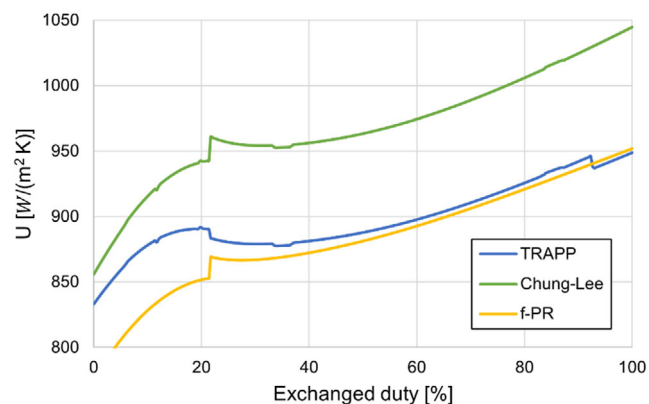
the marked decrease of the thermal conductivity, from the hot-in to the pinch-point, determines an overall progressive reduction of the convective heat transfer coefficient in the LP side. On the other hand, the TRAPP model provides a higher thermal conductivity but at the same time higher viscosity compared with the fitted f-PR model. As a consequence, the resulting heat transfer coefficients are quite similar using the two models especially in the single-phase region, while notable difference can be seen in the two-phase region. In the end, the resulting recuperator design with the two models is very similar because the two-phase field corresponds only at about 20% of the total exchanged thermal power. While the Chung–Lee–Starling model estimates a higher thermal conductivity and, at the same time, a similar or even lower viscosity compared to the f-PR model, leading to a more compact PCHE. The design results are reported in **Table 10**.

The cycle power balance and PCHE design, using f-PR, at different hot-side percentage pressure drop, keeping a constant net mechanical output, are reported in **Table 11**. The different PCHE design affects both the upper and the lower isobars. The pump inlet pressure is fixed to achieve saturation conditions at 51 °C, while the pressure at turbine inlet is set as constant parameter at 250 bar. Thus, the different pressure drops in the HP and LP streams of the recuperator affect both the pump outlet and the turbine outlet conditions. When the allowable pressure drop in the PCHE channel increases, also the channel length increases due to more duty exchanged in the single channel, even if the heat transfer coefficients are higher.

The LCOE is so computed to see the impact of the PCHE design at different pressure drops on the overall CSP plant. The cost functions to assess the capital costs of the power block are taken from Weiland et al.[61] for turbine, pump, motor, and generator, whereas Thermoflex has been used to determine the cost of the PHE. The economic analysis is carried out installing the power block and the CSP tower in Sevilla (Spain). The cost functions of the solar tower, receiver, HTF pump, and piping are taken from Kelly et al.,[62] while the solar field cost is assumed equal to 145 \$ m^{-2} of heliostat area as suggested in System Advisor Model.[63] An 8-hours TES, which consists of two molten salts tanks, is assumed computing the related cost from the work of Manzolini et al.[64] The design of the solar field, for a thermal input of 717 MW$_{th}$ at the receiver, as well as additional financial
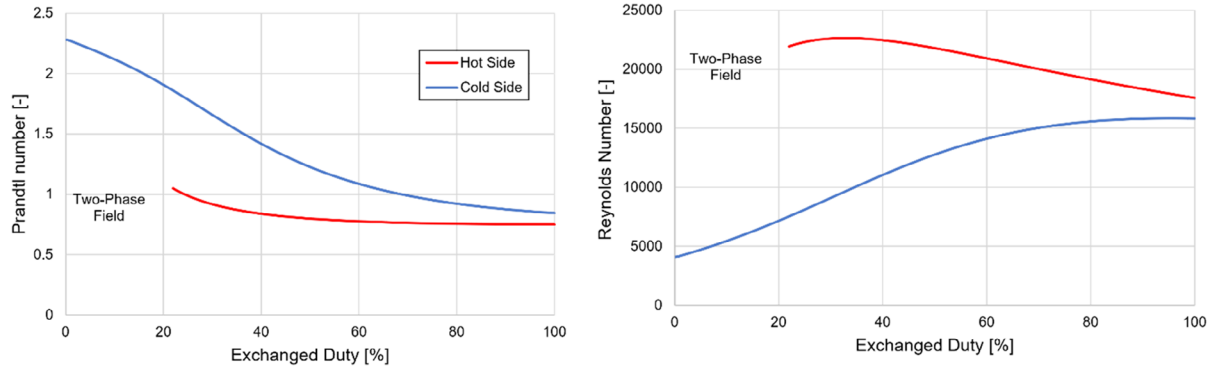

Figure 16. Mixture $CO_2 + C_6F_6$: U along the PCHE, model comparison (base case).

Figure 17. Mixture $CO_2 + C_6F_6$: Prandtl and Reynolds numbers trend along the PCHE.

Table 10. Mixture $CO_2 + C_6F_6$: PCHE design results (base case).

	TRAPP	f-PR	Chung-Lee
G [kg s m^{-2}]	432	429	449
$N_{ch,hot/cold} \times 10^6$	1.8	1.82	1.74
L_z [m]	4.07	4.15	3.97
A [m^2]	37'800	38'780	35'267
V [m^3]	76.4	78.4	71.3
Cost [M\$]	28.1	28.8	26.2

and operating expenses related to the CSP plant, is presented in ref. [65]. The LCOE is calculated as

$$\text{LCOE} \left[\frac{\$}{\text{MWh}_{el}} \right] = \frac{\text{CSP Plant CAPEX} \cdot \text{CRF} + \text{CSP Fixed OPEX}}{\text{Yearly Net Electric Energy Produced}}$$
$$+ \text{CSP Variable OPEX}$$

$$(38)$$

Table 12 reports the capital cost related to the components of the power block. The overall power block cost decreases as the allowable pressure drop across the PCHE increases, but at the same time, the size of the other power block components slightly increases at fixed 100 MW electrical output. The solar field and the tower are fixed, while the TES size is computed for each power cycle based on the optimal LCOE condition. An optimal TES size of 8 h is found, and the dimensions of the tanks to provide the design thermal have a low impact on the capital costs from one case to another. The results of the annual analysis considering Sevilla as location of the CSP plants with different power block and TES design are represented in **Table 13**.

As highlighted in **Figure 18**, a local minimum of the LCOE is found around a hot-side pressure drop of 3% due to a more compact PCHE with respect to the base case without affecting much the cycle efficiency (Table 11). The LCOE local minimum is not very significative, but it is relevant for many aspects: lower investment cost compared to the base case, lower number of PCHE modules operating in parallel reducing the risks of maldistribution, lower block welding and associated labor, and lower maintenance costs. When the available solar power exceeds the power block thermal input, the TES stores the exceeding energy until its

Table 11. Mixture $CO_2 + C_6F_6$: cycle performance at different PCHE pressure drop using f-PR as transport properties model.

Parameter	Units	1% $\Delta P_{H,rec}$	2% $\Delta P_{H,rec}$	3% $\Delta P_{H,rec}$	4% $\Delta P_{H,rec}$
$\Delta P_{C,rec}$[a]	bar	0.23	0.45	0.68	0.92
$\dot{m}$	kg s^{-1}	1224.7	1237.7	1251.3	1265.3
W_{pump}	MW	25.4	25.7	26.0	26.4
Q_{rec}	MW	609.4	617.0	624.9	629.1
$Q_{TH,in}$	MW	237.7	239.1	240.5	242.0
W_{turb}	MW	125.4	125.7	126.0	126.4
Q_{cond}	MW	137.7	139.1	140.5	142
UA_{PCHE}	MW K^{-1}	33.3	33.7	34.1	34.5
ϵ_{rec}	%	92.85	92.88	92.92	92.96
η_{cycle}	%	42.1	41.8	41.6	41.3
G	kg (sm^2)$^{-1}$	429	602	737	850
$N_{ch,hot/cold} \times 10^6$	–	1.82	1.31	1.08	0.95
L_z	M	4.15	4.49	4.65	4.76
A	m^2	35'267	30'218	25'836	23'193
V	m^3	78.4	61.1	52.2	46.9
Cost	M\$	28.8	22.4	19.2	17.2

[a]The pressure drop in the cold side of the recuperator is in accordance with the results of the design.

Table 12. Mixture $CO_2 + C_6F_6$: power block capital costs at different PCHE recuperator design.

PB costs	Units	1% $\Delta P_{H,rec}$	2% $\Delta P_{H,rec}$	3% $\Delta P_{H,rec}$	4% $\Delta P_{H,rec}$
Pump	M\$	4.85	4.89	4.94	5
Turbine	M\$	3	3.02	3.04	3.07
PHE	M\$	24.2	24.5	24.7	25
Condenser	M\$	8.78	8.86	8.91	9
Power Block	M\$	74.5	68.6	65.8	64.3
PCHE/PowerBlock	%	38.6	32.7	29.1	26.7

capacity is saturated and defocusing of the heliostats is practiced. The adoption of a more compact PCHE recuperator represents a good solution also because defocusing hours are reduced.

**ADVANCED
SCIENCE NEWS**

www.advancedsciencenews.com

Energy Technology
Generation, Conversion, Storage, Distribution

www.entechnol.de

Table 13. Mixture $CO_2 + C_6F_6$: annual analysis of the CSP plant at different recuperator design.

| CSP Plant results	Units	1% $\Delta P_{H,rec}$	2% $\Delta P_{H,rec}$	3% $\Delta P_{H,rec}$	4% $\Delta P_{H,rec}$
Yearly Electric Energy	$GWh_{el}\,year^{-1}$	407.5	405.45	404.07	401.98
Equivalent Hours of Defocusing	$h\,year^{-1}$	77	68	61	52
Solar Multiple	–	2.52	2.5	2.49	2.47
TES Cost	M$	60.11	60.5	60.76	61.16
Solar Field Cost	M$	183	183	183	183
Tower Cost	M$	24	24	24	24
Specific CSP CAPEX	$\,kW_{el}^{-1}$	5330	5262	5231	5218
PCHE % Investment Cost	–	5.5	4.3	3.7	3.4
LCOE	$\,MWh_{el}^{-1}$	133.9	133.1	132.9	133.3
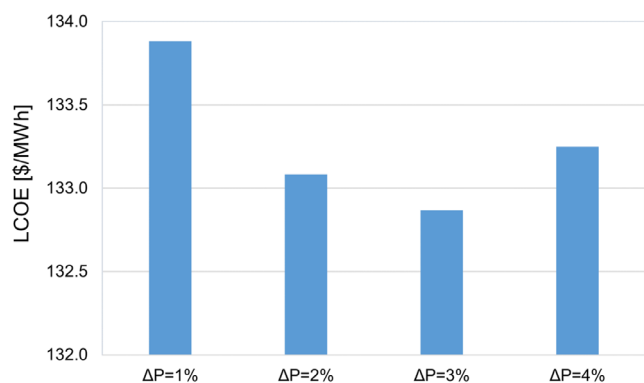
Figure 18. Mixture $CO_2 + C_6F_6$: LCOE of simple recuperated 100 MW cycle at different PCHE design conditions.

7. Conclusions

Over the last years, new closed power cycle configurations adopting CO_2-based mixtures as innovative working fluid are considered as promising alternative to sCO_2 cycles when dry cooling in hot environments is performed. In particular, some works suggested the use of CO_2 mixture with heavy and complex compounds, such as $CO_2 + C_6F_6$, in simple recuperative transcritical power cycle. Although preliminary analysis highlighted the benefits of this solution, a detailed design of the power block components requires the knowledge of the thermophysical properties of binary mixtures of interest. Previous literature works focused only on thermodynamic assessment of the CO_2-based mixture, but neither theoretical nor experimental studies on the transport properties have been performed. Starting from an extensive literature review, this work explored the adoption of suitable transport properties models for the design of the heat exchangers of the cycle, focusing on the PCHE recuperator of the transcritical power cycle with the $CO_2 + C_6F_6$ and $CO_2 + C_{10}H_{22}$ mixtures.

In general, the comparison of most appropriate models with available experimental data of CO_2-based mixtures highlights the shortcomings of the properties in the nonequilibrium field with respect to thermodynamics. On the other hand, the adoption of the recent friction theory model results to be a valid tool for modeling the transport properties from the dilute region to dense fluid states, even for asymmetric mixtures, compared to corresponding state-based models available in commercial software. Moreover, the f-theory models can be optimized on the pure component experimental data, without needing for binary interaction parameters, and this is a great benefit since experimental data of CO_2 mixtures are scarce especially in the HP conditions of a transcritical power cycle.

As there are no experimental data on the investigated $CO_2 + C_6F_6$ mixture, an additional CO_2 blend with a heavy dopant, $CO_2 + n$-decane, whose transport properties are well known, is selected to prove this concept. The two CO_2 mixtures have been investigated in optimized cycle conditions in concentrated solar power plants. The CO_2 mixture with n-decane showed a very high thermodynamic efficiency (32.5%) at 350 °C maximum temperature due to well-balanced heat capacities within the recuperator, in a simple-recuperated layout. On the other hand, the low mean temperature difference along the PCHE recuperator leads to a large heat transfer area and volume. Compared to TRAPP and Chung–Lee–Starling models, imported from commercial software, the adoption of the optimized friction theory model, implemented in an in-house code, proved to be effective in describing the heat transfer behavior of the mixture.

In case of the $CO_2 + C_{10}H_{22}$ mixture, the use the Chung–Lee model overpredicts the global heat transfer coefficient (around +16%), due to an underestimate of the dynamic viscosity. Instead, the heat transfer area obtained by the TRAPP method is similar to that obtained by the friction theory model (representative of real mixture behavior), even if the deviations in the transport properties prediction are marked: an overestimate of the viscosity by the TRAPP method entails lower Reynolds and Nusselt numbers, but it is compensated at the same time by an overestimate of thermal conductivity. This leads to comparable areas and volumes predicted by TRAPP and friction theory models.

The same outcome can be observed for the PCHE recuperator of the $CO_2 + C_6F_6$ mixture: compared to the optimized f-theory model, the TRAPP overestimate both viscosity and thermal conductivity, providing a similar heat transfer area and volume. Even if the TRAPP and Chung-Lee models are recognized as equally valid in a wide density domain, this research shows that the TRAPP model provides reasonable results for the CO_2-based mixtures investigated in terms of heat transfer area and volumes, even if the transport property prediction is questionable as evidenced by the comparison with experimental data of the case studies. Obviously, the use of the latter model could be not suitable, for example, in the calculation of pressure losses in the pipes of the power plant. In any case, dedicated analysis should be performed for each specific CO_2 mixture investigated, and the use of the optimized friction theory model results to be a useful tool to improve the reliability of the design results.

A better understanding of the heat transfer behavior of CO_2 binary mixtures is not only crucial for the cycle design but also to predict the off-design performance, and this work provides useful guidelines when dealing with the design of the heat exchangers of a transcritical CO_2-based cycle.

The optimal design of the PCHE of the transcritical power cycle working with $CO_2 + C_6F_6$ applied in a CSP located in Sevilla is found to be around 3% hot-side pressure drop, a solution that allows more compactness (lower capital costs) without affecting much the cycle efficiency and reducing the maldistribution risks too.

Supporting Information

Supporting Information is available from the Wiley Online Library or from the author.

Conflict of Interest

The authors declare no conflict of interest.

Data Availability Statement

The data that support the findings of this study are available from the corresponding author upon reasonable request.

[1] Greenpeace, Solar Thermal Electricity, https://www.greenpeace.org/archive-international/Global/international/publications/climate/2016/Solar-Thermal-Electricity-Global-Outlook-2016.pdf (accessed: January 2023).

[2] SCARABEUS, *Supercritical Carbon Dioxide/Alternative Fluids Blends for Efficiency Upgrade of Solar Power Plants* **2019**, https://www.scarabeusproject.eu/.

[3] E. Morosini, M. Doninelli, D. Alfani, M. Astolfi, G. Di Marcoberardino, G. Manzolini, in *Conf. Proc. European SCO₂ Conf.*, Prague, Czech Republic **2023**, pp. 169–178, https://doi.org/10.17185/duepublico/77287.

[4] G. Di Marcoberardino, E. Morosini, G. Manzolini, *Energy* **2022**, *238*, 121815.

[5] E. M. S. Lasala, P. Chiesa, in *Conf. Proc. JEEP2014 – 40ième Journées d'Etudes Des Equilibres Entre Phases,* Lyon, France **2014**, pp. 10–11, https://doi.org/10.13140/RG.2.2.14853.58084.

[6] G. Di Marcoberardino, E. Morosini, D. Di Bona, P. Chiesa, C. Invernizzi, P. Iora, G. Manzolini, *Appl. Therm. Eng.* **2022**, *212*, 118520.

[7] E. Morosini, A. Ayub, G. di Marcoberardino, C. M. Invernizzi, P. Iora, G. Manzolini, *Energy Convers. Manage.* **2022**, *255*, 115263.

[8] G. Manzolini, M. Binotti, D. Bonalumi, C. Invernizzi, P. Iora, *Sol. Energy* **2019**, *181*, 530.

[9] H. Li, Ø. Wilhelmsen, Y. Lv, W. Wang, J. Yan, *Review of Available Experimental Data and Models for the Transport Properties of CO₂-Mixtures Relevant For CO₂ Capture, Transport and Storage* **2011**, https://www.scarabeusproject.eu/.

[10] M. Nazeri, A. Chapoy, R. Burgass, B. Tohidi, *J. Chem. Thermodyn.* **2018**, *118*, 100.

[11] Z. Liu, B. Liu, J. Guo, X. Xin, X. Yang, *Energy Convers. Manage.* **2019**, *198*, 111807.

[12] L. Chai, S. A. Tassou, *Therm. Sci. Eng. Prog.* **2020**, *18*, 100543.

[13] S. Li, Z. Zhao, Y. Zhang, H. Xu, W. Zeng, *Energies* **2020**, *13*, 6589 .

[14] I. H. Kim, H. C. No, *Exp. Therm. Fluid Sci.* **2013**, *48*, 213.

[15] R. B. Bird, W. E. Stewart, E. N. Lightfoot, *AIChE J.* **1961**, *7*, 5J.

[16] T. H. Chung, L. L. Lee, K. E. Starting, *Ind. Eng. Chem. Fundam.* **1984**, *23*, 8.

[17] B. E. Poling, J. M. Prausnitz, *The Properties of Gases and Liquids* **2001**, https://www.scarabeusproject.eu/.

[18] C. R. Wilke, *J. Chem. Phys.* **1950**, *18*, 517.

[19] A. Wassiljewa, *Phys. Z* **1904**, *5*, 737.

[20] E. A. Mason, S. C. Saxena, *J. Chem. Phys.* **1959**, *31*, 511.

[21] T. H. Chung, M. Ajlan, L. L. Lee, K. E. Starling, *Ind. Eng. Chem. Res.* **1988**, *27*, 671.

[22] D. Browarzik, J. P. M. Trusler, I. G. Economou, J. Ely, C. McCabe, A. Galindo, M. A. Anisimov, M. C. Kroon, E. Lemmon, S. Bottini, E. Brignole, S. Pereda, S. Kjelstrup, D. Bedeaux, S. I. Sandler, *Applied Thermodynamics of Fluids*, The Royal Society of Chemistry, Cambridge, England **2011**, https://doi.org/10.1039/9781849730983.

[23] J. W. Leach, P. S. Chappelear, T. W. Leland, *AIChE J.* **1968**, *14*, 568.

[24] E. W. Lemmon, I. H. Bell, M. L. Huber, M. O. McLinden, *NIST Standard Reference Database 23: Reference Fluid Thermodynamic and Transport Properties-REFPROP, Version 10.0*, National Institute of Standards and Technology, Gaithersburg, U.S.A **2018**, https://doi.org/10.18434/T4/1502528.

[25] M. L. Huber, D. G. Friend, J. F. Ely, *Fluid Phase Equilib.* **1992**, *80*, 249.

[26] W. D. Monnery, A. K. Mehrotra, W. Y. Svrcek, *Can. J. Chem. Eng.* **1991**, *69*, 1213.

[27] S. E. Quiñones-Cisneros, C. K. Zéberg-Mikkelsen, E. H. Stenby, *Fluid Phase Equilib.* **2001**, *178*, 013102.

[28] J. F. Ely, H. J. M. Hanley, *A Computer Program for the Prediction of Viscosity and Thermal Conductivity in Hydrocarbon Mixtures* **1981**, https://www.scarabeusproject.eu/.

[29] B. A. Younglove, J. F. Ely, *J. Phys. Chem. Ref. Data* **1987**, *16*, 577.

[30] J. F. Ely, *J. Res. Natl. Bur. Stand.* **1981**, *86*, 597.

[31] M. L. Huber, E. A. Sykioti, M. J. Assael, R. A. Perkins, *J. Phys. Chem. Ref. Data* **2016**, *45*, 013102.

[32] P. L. Christensen, A. A. Fredenslund, *Chem. Eng. Sci.* **1980**, *35*, 871.

[33] S. E. Quiñones-Cisneros, U. K. Deiters, *J. Phys. Chem. B* **2006**, *110*, 12820.

[34] S. E. Quiñones-Cisneros, S. Pollak, K. A. G. Schmidt, *J. Chem. Eng. Data* **2021**, *66*, 4215.

[35] The MathWorks Inc., *MATLAB* **2022a**, https://www.scarabeusproject.eu/.

[36] F. F. Czubinski, C. J. Noriega Sanchez, A. K. Da Silva, M. A. Marcelino Neto, J. R. Barbosa, *J. Chem. Eng. Data* **2019**, *64*, 3375.

[37] J. Pátek, J. Klomfar, L. Čapla, P. Buryan, *Int. J. Thermophys.* **2005**, *26*, 577.

[38] D. Kim, S. W. Løvseth, A. Arami-Niya, E. F. May, *J. Chem. Eng. Data* **2021**, *66*, 4018.

[39] K. Kian, A. M. Scurto, *Ind. Eng. Chem. Res.* **2017**, *56*, 12822.

[40] Aspen Technology Inc., *Aspen Plus, Version V12.1* **2022**, https://www.scarabeusproject.eu/.

[41] C. K. Zeberg-Mikkelsen, E. H. Stenby, *Viscosity Study of Hydrcarbon Fluids at Reservoir Conditions Modeling and Measurements* **2001**, https://www.scarabeusproject.eu/.

[42] X. Zheng, D. Qu, F. Zhang, Y. Liu, G. Qin, *Fluid Phase Equilib.* **2021**, *533*, 112940.

[43] M. G. Freire, A. G. M. Ferreira, I. M. A. Fonseca, I. M. Marrucho, J. A. P. Coutinho, *J. Chem. Eng. Data* **2008**, *53*, 538.

[44] J. H. Dymond, J. Robertson, J. D. Isdale, *Int. J. Thermophys.* **1981**, *2*, 223.

[45] J. B. Irving, D. T. Jamieson, *J. Fluorine Chem.* **1975**, *5*, 449.

[46] J. F. Counsell, J. H. S. Green, J. L. Hales, J. F. Martin, *Trans. Faraday Soc.* **1965**, *61*, 212.

[47] R. Le Pierres, D. Southall, S. Osborne, in *Proc. SCO₂ Power Cycle Symp.*, Boulder, U.S.A **2011**, pp. 24–25.

[48] A. P. Simanjuntak, J. Y. Lee, *Appl. Sci.* **2020**, *10*, 2169.

[49] Y. Jiang, E. Liese, S. E. Zitney, D. Bhattacharyya, *Appl. Energy* **2018**, *231*, 1019.

[50] ASME, *An International Code 2015 ASME Boiler & Pressure Vessel Code Section III. Rules for Construction of Nuclear Facility Components Division 5 High Temperature Reactors*, New York, NY **2015**.

[51] T. W. Watson, H. E. Robinson, *Thermal Conductivity of a Sample of SS 316*, **1963**, https://www.scarabeusproject.eu/.

[52] S. J. Dewson, C. Grady, *HEATRICTM Workshop at MIT*, https://www.scarabeusproject.eu/.

[53] Chemical Engineering Magazine, n.d., https://www.chemengonline.com/tag/cepci/

[54] V. Dostal, P. Hejzlar, M. J. Driscoll, *Nucl. Technol.* **2006**, *154*, 265.

[55] S. Chung, S. W. Lee, N. Kim, S. M. Shin, M. H. Kim, H. J. Jo, *Appl. Therm. Eng.* **2023**, *218*, 119348.

[56] V. Illyés, E. Morosini, M. Doninelli, P.-L. David, X. Guerif, A. Werner, G. Di Marcoberardino, G. Manzolini, *Design of An Air-Cooled Condenser for CO₂-Based Mixtures: Model Development, Validation and Heat Exchange Gain with Internal Microfins*, **2022**, p. V009T28A016, https://doi.org/10.1115/GT2022-82438.

[57] F. Crespi, P. Rodríguez de Arriba, D. Sánchez, A. Ayub, G. Di Marcoberardino, C. M. Invernizzi, G. S. Martínez, P. Iora, D. Di Bona, M. Binotti, G. Manzolini, *Energy* **2022**, *238*, 121899.

[58] F. Crespi, G. S. Martínez, P. R. De Arriba, D. Sánchez, F. Jiménez-Espadafor, *Proc. ASME Turbo Expo* **2021**, *10*, 013102.

[59] O. A. Aqel, M. T. White, M. A. Khader, A. I. Sayma, *Appl. Therm. Eng.* **2021**, *190*, 116796.

[60] H. Knapp, S. Zeck, R. Langhorst, *Vapor-Liquid Equilibria for Mixtures of Low Boiling Substances. Pt. 3. Ternary Systems*, Frankfurt am Main, Germany, FR; Dechema, Germany **1989**.

[61] N. T. Weiland, B. W. Lance, S. R. Pidaparti, *SCO₂ Power Cycle Component Cost Correlations from DOE Data Spanning Multiple Scales and Applications* **2019**, https://doi.org/10.1115/GT2019-90493.

[62] B. Kelly, M. Izygon, L. Vant-Hull, in *SolarPaces Conf.*, U.S.A **2010**, https://doi.org/10.2172/981926.

[63] System Advisor Model (SAM), n.d., https://sam.nrel.gov/

[64] G. Manzolini, G. Lucca, M. Binotti, G. Lozza, *Renewable Energy* **2021**, *177*, 807.

[65] M. Doninelli, E. Morosini, G. Gentile, L. Putelli, G. Di Marcoberardino, M. Binotti, G. Manzolini, *Sustainable Energy Technol. Assess.* **2023**, *60*, 103481.

[66] B. Zohuri, *Compact Heat Exchangers: Selection, Application, Design and Evaluation* **2016**, https://doi.org/10.1007/978-3-319-29835-1.

[67] J. Kestin, W. Leidenfrost, C. Liu, *Z. Angew. Math. Phys.* **1959**, *10*, 558.

[68] K. J. Dewitt, G. Thodos, *Can. J. Chem. Eng.* **1966**, *44*, 148.

[69] D. E. Diller, L. J. Van Poolen, F. V. dos Santos, *J. Chem. Eng. Data* **1988**, *33*, 460.

[70] A. S. Culllck, M. L. Mathis, *J. Chem. Eng. Data* **1984**, *29*, 393.

[71] A. I. Johns, A. C. Scott, J. T. R. Watson, D. Ferguson, A. A. Clifford, *Philos. Trans. R. Soc. London, Ser. A* **1988**, *325*, 295.

[72] N. Imaishi, J. Kestin, W. A. Wakeham, R. Island, *Introduction* **1984**, pp. 50–71, https://www.scarabeusproject.eu/.